LIMNOLOGY
and
OCEANOGRAPHY

ASLO

Limnol. Oceanogr. 61, 2016, 1661–1676

doi: 10.1002/lno.10324

Silicon and nitrogen cycling in the upwelling area off Peru: A dual isotope approach

Patricia Grasse,*[1] Evgenia Ryabenko,[2] Claudia Ehlert,[3] Mark A. Altabet,[4] Martin Frank[1]

[1]GEOMAR Helmholtz Center for Ocean Research Kiel, Ocean Circulation and Climate Dynamics, Kiel, Germany
[2]Helmholtz Center Munich, Institute for Groundwater Ecology, Neuherberg, Germany
[3]Max Planck Research Group for Marine Isotope Geochemistry, Institute for Chemistry and Biology of the Marine Environment (ICBM), University of Oldenburg, Oldenburg, Germany
[4]School for Marine Science and Technology (SMAST), Department of Estuarine and Ocean Sciences, University of Massachusetts Dartmouth, New Bedford, Massachusetts

Abstract

We present a comparison of the dissolved stable isotope composition of silicate ($\delta^{30}Si(OH)_4$) and nitrate ($\delta^{15}NO_3^-$) to investigate the biogeochemical processes controlling nutrient cycling in the upwelling area off Peru, where one of the globally largest Oxygen Minimum Zones (OMZs) is located. Besides strong upwelling of nutrient rich waters mainly favoring diatom growth, an anticyclonic eddy influenced the study area. We observe a tight coupling between the silicon (Si) and nitrogen (N) cycles in the study area. Waters on the shelf showed high $Si(OH)_4$ concentrations accompanied by diminished NO_3^- concentration as a consequence of intense remineralization, high Si fluxes from the shelf sediments, and N-loss processes such as anammox/denitrification within the OMZ. Correspondingly, the surface waters show low $\delta^{30}Si(OH)_4$ values (+2‰) due to low Si utilization but relatively high $\delta^{15}NO_3^-$ (+13‰) values due to upwelling of waters influenced by N-loss processes. In contrast, as a consequence of the deepening of the thermocline in the eddy center, a pronounced $Si(OH)_4$ depletion led to the highest $\delta^{30}Si(OH)_4$ values (+3.7‰) accompanied by high $\delta^{15}NO_3^-$ values (+16‰). In the eddy center, high NO_3^-: $Si(OH)_4$ ratios favored the growth of non-siliceous organisms (*Synechococcus*). Our data show that upwelling processes and the presence of eddies play important roles controlling the nutrient cycles and therefore also exert a major influence on the phytoplankton communities in the Peruvian Upwelling. Our findings also show that the combined approach of $\delta^{30}Si(OH)_4$ and $\delta^{15}NO_3^-$ can improve our understanding of paleo records as it can help to disentangle utilization and N-loss processes.

Introduction

The upwelling area off Peru is characterized by extremely high primary productivity (Thiede and Suess, 1983; Berger et al., 1989; Pennington et al., 2006) and one of the globally largest Oxygen Minimum Zones (OMZs) with oxygen levels below 5 μmol L^{-1} mainly between 100 m and 500 m water depth (Karstensen et al., 2008; Fuenzalida et al., 2009). The extent and strength of the OMZ is a function of ventilation via ocean circulation and degradation of organic matter depending on primary productivity in the euphotic zone, which is driven by upwelling, and exerts major influence on nutrient cycling. The high productivity close to the shelf is mainly induced by upwelling of subsurface waters with high phosphate (PO_4^{3-}), silicic acid ($Si(OH)_4$), and iron (Fe) concentrations (Bruland et al., 2005). Besides strong surface and subsurface currents, eddies are reoccurring hydrographic features in the area off Peru (Chaigneau et al., 2008; Stramma et al., 2013), which have a strong influence on the local biogeochemical cycles. A model study of eastern boundary upwelling systems by Gruber et al. (2011) suggested that high eddy activity is associated with low levels of biological production, leading to reduced export of organic matter. This is in contrast to other studies in the open ocean, which came to the conclusion that eddies lead to enhanced productivity due to intrusion of nutrients into surface waters (e.g., McGillicuddy et al., 1998). In general, cyclonic eddies and mode water eddies inject nutrients from below into the euphotic zone, while anticyclonic eddies decrease the nutrient content of the euphotic zone, which has also implications on the phytoplankton communities (e.g., Thompson et al., 2007; Bibby and Moore et al., 2011; Stramma et al., 2013). The dominant phytoplankton species in the

*Correspondence: pgrasse@geomar.de

Additional Supporting Information may be found in the online version of this article.

upwelling region are diatoms (Estrada and Blasco, 1985; Franz et al., 2012), which require $Si(OH)_4$ to form their biogenic silica ($bSiO_2$) shells (Lewin, 1961) and which contribute approximately 75% to the primary production in coastal and nutrient rich zones (Nelson et al., 1995). In contrast, the offshore regions in the Eastern Equatorial Pacific (EEP) are rather characterized by high nutrient, low chlorophyll (HNLC) conditions (Strickland et al., 1969; Thomas, 1979) and are dominated by non-siliceous organisms, such as the cyanobacteria *Synechococcus* and *Prochlorococcus* (Franz et al., 2012). Phytoplankton uses both new and recycled nitrogen in the form of different N-species including nitrate (NO_3^-), nitrite (NO_2^-), and ammonia (NH_4^+), whereby uptake of NH_4^+ is associated with the lowest energetic expenses. In general the Si and N cycle in upwelling areas is tightly coupled. Diatoms normally incorporate NO_3^- and $Si(OH)_4$ at a 1 : 1 ratio (Brzezinski 1985; Ragueneau et al., 2000), but stress, such as Fe limitation can lead to an enhanced uptake of $Si(OH)_4$ relative to NO_3^- resulting in heavier silicified frustules of the diatoms (Hutchins and Bruland, 1998; Franck et al., 2000). Therefore, the deviation from the 1 : 1 NO_3^- to $Si(OH)_4$ ratio can serve as an indicator for the degree of utilization of NO_3^- over $Si(OH)_4$. A higher relative utilization of $Si(OH)_4$ is consequently reflected by higher $NO_3^-/Si(OH)_4$ (N/Si) ratios resulting in either less silicified diatoms or even enhanced prevalence of non-siliceous organisms (Conley and Malone 1992; Wilkerson and Dugdale, 1996).

Biological processes controlling present and past Si and N cycling in the upwelling area off Peru are traceable by their stable isotope distributions in the water column. They can be used for example, as indicators for utilization processes because the lighter isotopes are preferentially incorporated into the organisms (e.g., Montoya and McCarthy, 1995; De LaRocha et al., 1997). In general, the biogeochemical processes are accompanied by specific fractionation factors (e.g., Mariotti et al., 1981) and can be expressed as offset (Δ), where the isotopic composition (IC) of the source (e.g., the $Si(OH)_4$ in seawater) is subtracted from the IC of the product (e.g., a diatom) or as the fractionation factor α, where the IC of the product is divided by the IC of the source.

$$\Delta = \delta_{\text{Product}} - \delta_{\text{Source}} \quad (1)$$

$$\alpha = \frac{\delta_{\text{Product}}}{\delta_{\text{Source}}} \quad (2)$$

For an easier handling, α is often expressed as the enrichment factor (ε):

$$\varepsilon = (\alpha - 1) * 1000 \quad (3)$$

Literature on N isotope biogeochemistry commonly uses inverse fractionation factors, resulting in $\alpha > 1$ and therefore positive enrichment factors. In the following, we will use the relationships (2) and (3), which are commonly used in Si isotope literature.

The isotope composition of Si is fractionated during incorporation into diatom shells with an enrichment factor ($^{30}\varepsilon$) of $-0.5‰$ to $-2.1‰$ (De La Rocha et al., 1997; Milligan et al. 2004; Sutton et al., 2012), which leaves the surrounding seawater enriched in the heavy isotopes. It is still under discussion if there is also a fractionation during dissolution of $bSiO_2$ material. A laboratory study by Demarest et al. (2009) indicated a fractionation with the release of lighter isotopes into solution, whereas a more recent study by Wetzel et al. (2014) was not able to confirm fractionation during diatom dissolution. Thus, the Si isotope distribution in oceanic waters is mainly controlled by utilization in the surface waters, remineralization and water mass mixing (e.g., Reynolds et al., 2006; Grasse et al., 2013).

Laboratory studies have shown that the utilization of NO_3^- by phytoplankton is highly variable with enrichment factors ($^{15}\varepsilon$) ranging from $-1‰$ to $-20‰$ with no clear relationship between different marine species (e.g., Montoya & McCarthy, 1995; Needoba et al., 2003; Granger et al., 2004, 2010). In contrast, field studies generally obtained lower $^{15}\varepsilon$ of approximately -5 to $-10‰$, with most estimates closed to $-5‰$ (e.g., Wada, 1980; Altabet, 2001).

In OMZs, a number of additional processes occur that influence the dissolved N isotope composition. Low oxygen concentrations (2 to 10 μmol L^{-1}) induce N-loss processes, such as denitrification ($NO_3^- \rightarrow NO_2^- \rightarrow NO \rightarrow N_2O \rightarrow N_2$) and/or the more direct anammox (ANaerobic AMMonium OXidation) process ($NH_4^+ \rightarrow NO_2^- \rightarrow N_2$; Codispodi, 2007; Lam et al., 2009; Kalvelage et al., 2013). Another NO_3^- reducing process is the dissimilatory reduction of NO_3^- to NH_4^+ (DNRA), which also occurs under anaerobic conditions. NO_3^- reduction is known to result in both strong N as well as O isotopic fractionation ($\varepsilon\ ^{15}N = -20‰$ to $-30‰$; e.g., Granger et al., 2008; Casciotti, 2009) leaving residual seawater NO_3^- enriched and produce isotopically light ^{15}N products (Casciotti and McIlvin, 2007). There are also processes that regenerate bioavailable N, like N_2 fixation by cyanobacteria and *in situ* regeneration of N via nitrification ($NH_4^+ \rightarrow NO_2^- \rightarrow NO_3^-$; e.g., Deutsch et al., 2007; Fernández et al., 2009).

The above processes can also influence the $\delta^{15}N$ signature of the sedimentary record, given that supply of the heavy $\delta^{15}NO_3^-$ signatures of subsurface waters leads to particulate organic matter enriched in ^{15}N, which is ultimately buried in the sediments (e.g., Altabet and Francois, 1994; Altabet, 2006; Mollier-Vogel et al., 2012). Therefore, it is difficult to disentangle the influence of utilization and the N-loss signals, which can cause difficulties in the interpretation of paleo records (Mollier-Vogel et al., 2012). In contrast, Si isotopes are subject to a relatively simple cycling mainly influenced by utilization and subsequent dissolution of diatoms. An approach using a combination of both isotope systems will therefore be helpful to understand and reconstruct the marine biogeochemical cycles of nutrients in upwelling areas. For this purpose, it is crucial to understand the factors

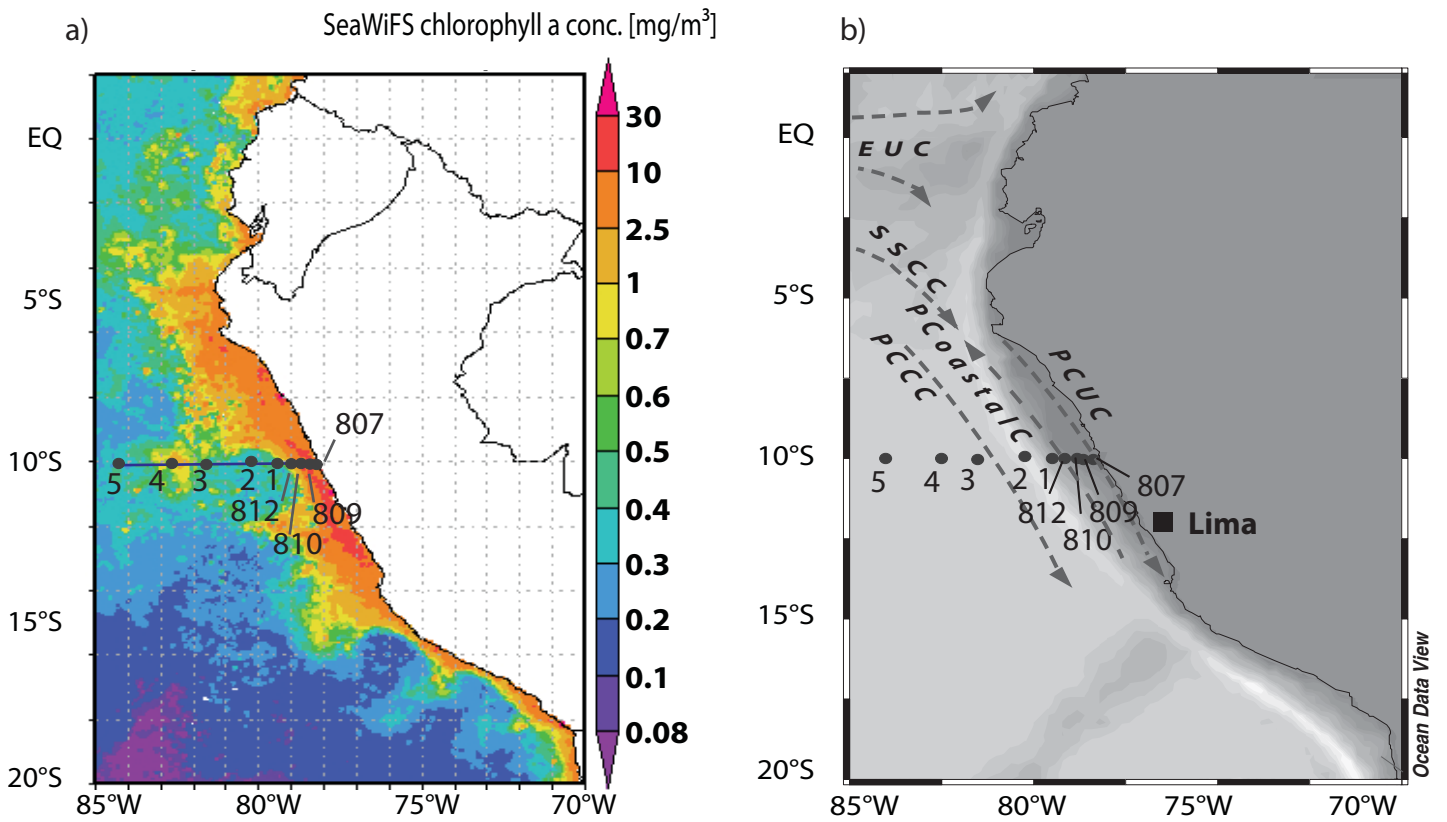

Fig. 1. (a) Sampling locations and Chlorophyll *a* concentrations (mg m^{-3}). Chlorophyll concentrations were obtained from the NASA Giovanni website (*http://disc.sci.gsfc.nasa.gov/giovanni/overview/index.html*) for January and February 2009. For Sta. 1 and Sta. 3, no Si isotope measurements were carried out. (b) Schematic subsurface currents (dashed gray lines) off Peru. (EUC: Equatorial Undercurrent, SSCC: Southern Subsurface Countercurrent, PCUC: Peru Chile Undercurent, PCCC: Peru-Chile Countercurrent, PCoastalC: Peru Coastal Current; according to Strub et al., 1998; Penven et al., 2005; Kessler, 2006; Ayon et al., 2008; Karstensen and Ulloa, 2008; and ADCP data according to Czeschel et al., 2011). [Color figure can be viewed in the online issue, which is available at wileyonlinelibrary.com.]

controlling the $Si(OH)_4$ and NO_3^- cycles and the supply of these nutrients to the euphotic zone, as well as primary productivity, remineralization processes, and water mass mixing.

Here, we present combined nutrient concentrations and stable isotope compositions of dissolved $Si(OH)_4$ and NO_3^-, as well as its oxygen isotope composition ($\delta^{18}O$-NO_3^-) and $\delta^{15}NO_2^-$ in the water column along a 10°S transect in the EEP off Peru influenced by strong upwelling on the shelf and the presence of an anticyclonic eddy. These data allow the investigation of the influence of the hydrographic settings on the Si and N cycles.

Material and methods

All samples were collected during cruise M77-3 with the German RV Meteor between end of December 2008 and January 2009 in the frame of the Collaborative Research Center (SFB) 754: Climate – Biogeochemistry Interactions in the Tropical Ocean. Seawater samples were collected along a 10°S transect perpendicular to the Peruvian Coast (Fig. 1, Table S1). Seawater samples for nutrient and oxygen concentration, as well as for Si and N isotope measurements were collected using a Seabird CTD Rosette System equipped with oxygen sensors. Oxygen concentrations were determined with the O_2-sensor of the CTD and were later calibrated with bottle data obtained by Winkler titration (Winkler, 1888). Samples for nutrient measurements were frozen (−20°C) on board immediately after sampling and were measured in the laboratory of the Max Planck Institute (MPI) for Marine Microbiology in Bremen with an autoanalyzer (TRAACS 800, Bran & Lubbe, Hamburg, Germany). Nutrient concentrations were measured following Grasshoff et al. (1999). $Si(OH)_4$ concentrations of the frozen samples were compared to selected filtered and acidified (non-frozen) samples. The reproducibility ranged between 5 and 10% (see also Ehlert et al., 2012). Concentrations of particulate organic nitrogen (PON), and $bSiO_2$ were adapted from Franz et al. (2012). Seawater samples for Si isotope measurements were immediately filtered on board through nitrocellulose acetate filters (0.45 μm pore size) and were then acidified with distilled HCl to pH 2. At GEOMAR Si was separated from the samples using a brucite-coprecipitation method (Reynolds et al., 2006; following Karl and Tien, 1992). Only samples with

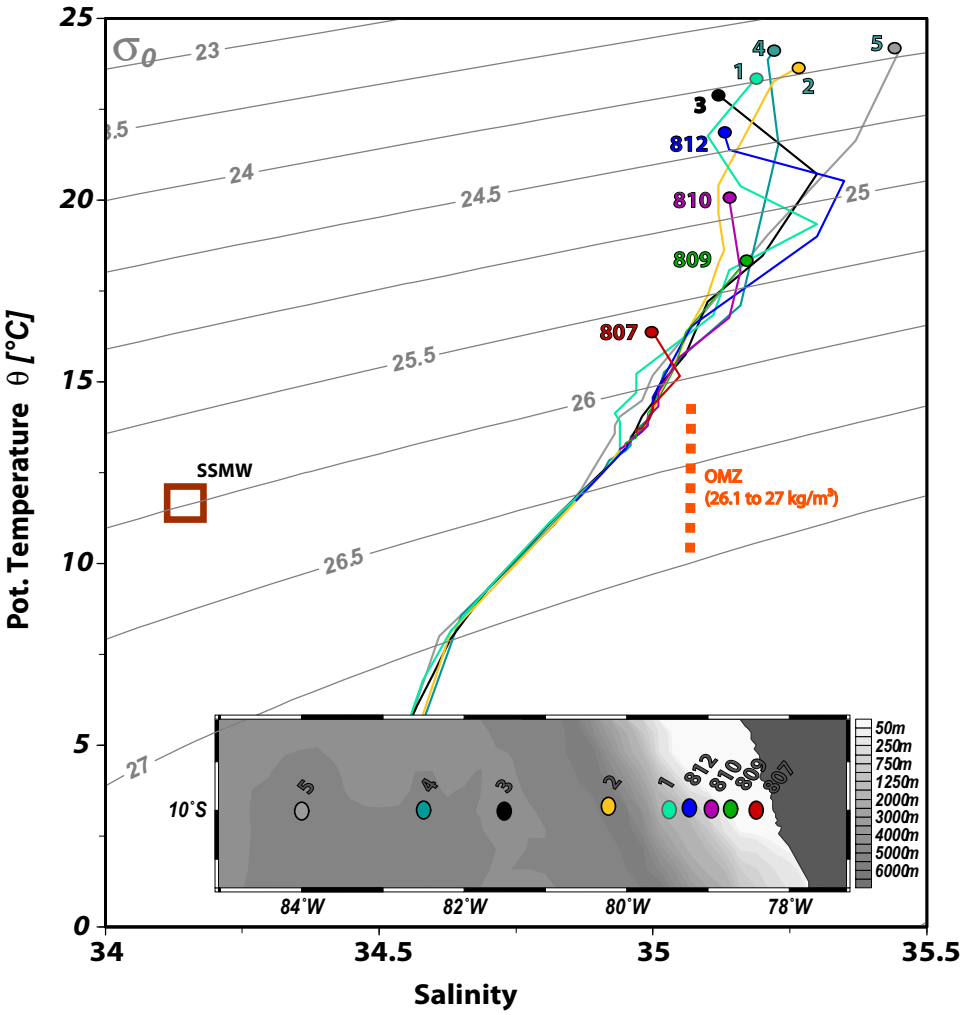

Fig. 2. Temperature-salinity (TS) plot for all stations with potential density isolines along the 10°S transect. The "Shallow Salinity Minimum Water" (SSMW) is defined by a salinity of 34.2 and a pot. density of 26 kg m^{-3} (red square; Reid 1973; Karstensen 2004). The extend of the OMZ is shown by the dashed orange line (26.1 kg m^{-3} and 27 kg m^{-3}). Deep water masses are not shown as only data in the upper 300m are discussed. For other water masses in the study area, see also Grasse et al. (2012). [Color figure can be viewed in the online issue, which is available at wileyonlinelibrary.com.]

yields >97% were accepted for isotopic measurements given that incomplete precipitation would lead to isotopic fractionation of the Si in the samples. For Si isotope measurements, samples were purified following the method by Georg et al. (2006) and measured on a *NuPlasma* MC-ICPMS (Nu instruments) at GEOMAR. For a detailed method description, see Ehlert et al. (2012) and Grasse et al. (2013). Si data for Station 807 were adapted from Ehlert et al. (2012).

Seawater samples for $\delta^{15}NO_3^-$, $\delta^{15}NO_2^-$ and $\delta^{18}O\text{-}NO_3^-$ analysis were collected in 125 mL HDPE bottles and kept frozen (−20°C) until analysis. Samples that contained low to negligible levels of nitrite (NO_2^- <0.1 μmol L^{-1}) were acidified and stored at room temperature after defrosting, whereas samples with significant NO_2^- contents were kept frozen prior to NO_2^- analysis. Aliquots of these samples were treated in the laboratory with sufficient sulfanic acid to remove NO_2^- prior to $^{15}NO_3^-$ analysis. Acidified samples do not show any storage effects given that repeat measurements of ^{15}N were constant over years (see also Ryabenko et al., 2012). The stable isotope composition of dissolved NO_3^- was measured using Cd-reduction to NO_2^- followed by reaction with azide to produce N_2O. This method makes it not only possible to measure the $\delta^{15}N$, but also the $\delta^{18}O$ of nitrate (McIlvin and Altabet, 2005). NaCl was added to ensure consistent quantitative yields (Ryabenko et al, 2009). Samples were analyzed at GEOMAR and the SMAST using a purge-trap isotope ratio mass spectrometer (PT-IRMS) system.

Si and N isotope compositions are reported in the δ notation representing the deviations of the measured isotope ratios of the samples from that of a reference standard in parts per thousand (‰):

$$\delta^{30}Si,\ \delta^{15}N,\ \delta^{18}O = \left(\left(\frac{R_{sample}}{R_{std}}\right) - 1\right) * 1000 \qquad (4)$$

R_{sample} represents the ratio of the measured $^{30}Si/^{28}Si$, $^{15}N/^{14}N$, and $^{18}O/^{16}O$ ratios whereas R_{std} denotes the isotope ratio of the reference standard. For Si isotopes, the NBS28 standard is used, N isotopes are given relative to the N isotope ratio of air, using international reference standards USGS 34, USGS 35, and IAEA 3 for calibration. The reference standard for oxygen isotopes is the Vienna Standard Mean Ocean Water (V-SMOW. Repeated measurements of an internal seawater matrix standard gave a long-term reproducibility of $\pm 0.2‰$ ($2\sigma_{sd}$, $n = 15$) for Si isotope measurements and $\pm 0.4‰$ ($2\sigma_{sd}$, $n = 33$) for N isotope measurements. $\delta^{18}O$-NO_3^- are generally reproducible within 1‰ (2sd).

Results

Hydrographic setting of the study area

The main subsurface currents influencing the Peruvian upwelling (Fig. 1b) are the southward flowing Peru-Chile Countercurrent (PCCC) and the Peru-Chile Undercurrent (PCUC). The PCUC flows very close along the shelf between 50 m and 150 m water depth and represents the main source for the coastal upwelling (Huyer et al., 1987; Karstensen and Ulloa, 2008). The PCUC is partly fed by the Equatorial Undercurrent (EUC) and the Southern Subsurface Countercurrent (SSCC), which supply oxygen-rich waters to the upwelling area (Brink et al., 1983; Toggweiler et al., 1991; Fiedler and Talley, 2006). The sampling locations on the shelf (Sta. 807, 809 and 810) were dominated by upwelled waters mainly derived from the southward flowing PCUC, as reflected by low sea surface temperatures (Fig. 2). The main northward flowing subsurface current influencing the sampling location is the Peru Coastal Current (PCoastalC) at distances of approximately 100 km to 300 km from the shore (Strub et al., 1998; Penven et al., 2005; Karstensen and Ulloa, 2008). Unfortunately no ADCP data are available for the 10°S transect. However, the velocity distribution along at 6°S and 14°S section were recorded in February 2009 during Meteor cruise M77-4 (Czeschel et al., 2011) and show that at the PCoastalC, advected from the south from approx. 77°W, 14°S to 82°W, 6°S. Flowing northward, the surface current were subducted to 150 m to 300 m water depth and mainly influenced nearshore Sta. 812. Sta. 1 and 5 show a salinity minimum at about 50 m to 100 m (26 kg m^{-3}; Fig. 2), which is also characterized by a $Si(OH)_4$ depletion resulting in an Si* of −30 ($Si^* = Si(OH)_4 - 16*PO_4^-$, Supporting Information Fig. A1). This salinity minimum is ascribed to the admixture of "Shallow Salinity Mode Water" (SSMW, also called Eastern South Pacific Intermediate Water [ESPIW]), which originates from sinking of subantarctic surface waters at about 45°S off the Chileanen Coast (Fig. 2; Reid, 1973; Karstensen, 2004).

In addition to the above currents, the complex hydrographic system off Peru is influenced by mesoscale eddies, which transport waters from the shelf offshore (Chaigneau et al., 2008; Altabet et al., 2012). During the time of sampling in January 2009, a large anticyclonic coastal eddy entraining upwelled subsurface shelf waters was present in the study area, clearly visible in the Sea Level Anomaly (SLA) data (Fig. 3). The eddy extended to a depth of approximately 700m (Altabet et al., 2012) and showed high surface chlorophyll a concentrations obtained from SeaWIFS satellite data at its periphery (~ 2.5 mg m^{-3} to 20 mg m^{-3}) and low concentrations in its center (~ 0.3 mg m^{-3} to 0.5 mg m^{-3}; Fig. 1). The inner diameter of the eddy structure amounted to approximately 300 km and elevated chlorophyll concentrations of the outer filament were detected up to a longitude of 82°W to 85°W corresponding to the location of Sta. 4 in the center of the filament and Sta. 5 on its edge, whereas Sta. 2 was located in the center of the East/West extent of the eddy, which is characterized by low chlorophyll concentrations. In relation to its North/South extent Sta. 2 was close the edge of the northern eddy filament. In the following, we categorized the different hydrographic areas along the 10°S transect into coastal stations (Sta. 807, 809, 810), nearshore stations (Sta. 812, 1), the Eddy center (Sta. 2), and the outer filament of the eddy including the offshore stations (Sta. 3, 4, 5).

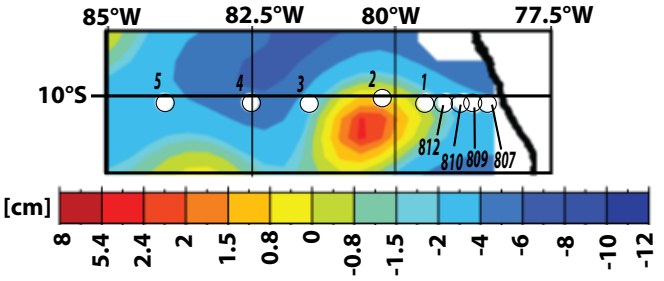

Fig. 3. Sea Level Anomaly (SLA) in cm along the 10°S Transect for January 2009 showing the extend of the eddy (adapted from http://www.aviso.oceanobs.com). The different hydrographic areas along the 10°S transect are divided into coastal stations (Sta. 807, Sta. 809, Sta. 810), nearshore stations (Sta. 812, Sta. 1), the Eddy center (Sta. 2), and the outer filament of the eddy including the offshore stations (Sta. 3, Sta. 4, Sta. 5). [Color figure can be viewed in the online issue, which is available at wileyonlinelibrary.com.]

Distribution of stable isotope compositions, nutrients, and oxygen concentrations along the 10°S transect

The distribution of dissolved $\delta^{30}Si(OH)_4$ and $\delta^{15}NO_3^-$, $\delta^{18}O$-NO_3^-, $\delta^{15}NO_2^-$, as well as of the nutrients and oxygen were analyzed for samples in the upper 300m of the water column along the 10°S transect (Figs. 4, Supporting Information Figs. A1, A2, Table S1). The depth of the oxycline varies between 20 m and 90 m (closely following a potential density of 26.1 kg m^{-3}) and is shallowest at Sta. 807 on the shelf and deepest at Sta. 2 in the center of the eddy. Below the oxycline, oxygen concentrations are essentially below 10 μmol L−, mostly at concentrations close to 0 μmol L^{-1} (Fig. 4a). The $\delta^{30}Si(OH)_4$ values in the water column range from + 1.1‰

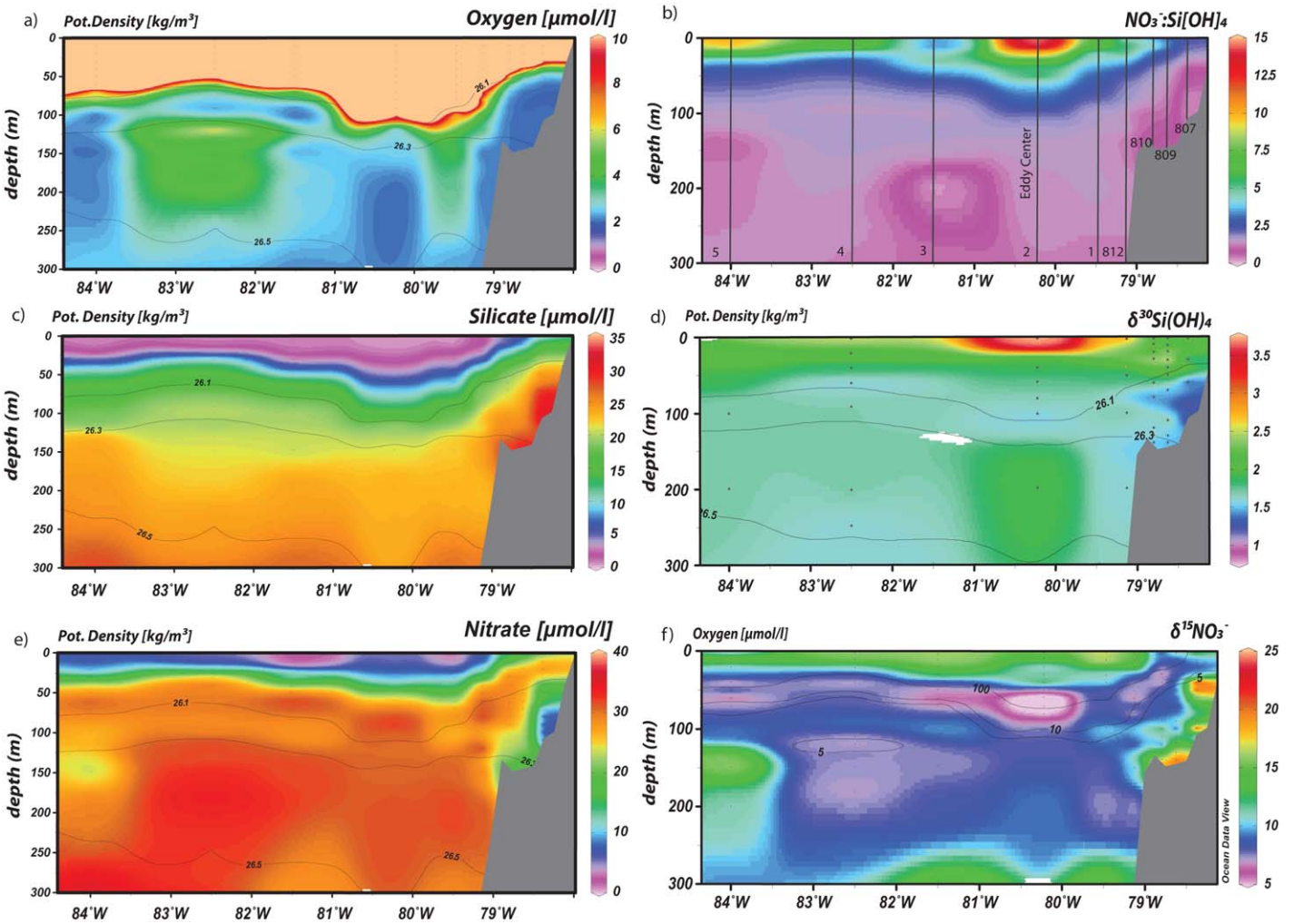

Fig. 4. Distribution of potential density (kg m^{-3}, contour lines) and oxygen concentrations (μmol L^{-1}, color) (a), NO_3^-: $Si(OH)_4$ ratios (b), $Si(OH)_4$ concentrations (μmol L^{-1} (c), $\delta^{30}Si(OH)_4$ (‰) (d), NO_3^- concentrations (μmol L^{-1}) (e), and $\delta^{15}NO_3^-$ (‰) (f) along the 10° transect. Locations of the sampling stations as well as the eddy center are marked with black lines in (b). [Color figure can be viewed in the online issue, which is available at wileyonlinelibrary.com.]

to + 3.7‰ while $Si(OH)_4$ concentrations range from 0.4 μmol L^{-1} at the surface to 32.7 μmol L^{-1} at depth (Figs. 4, 5). The highest $\delta^{30}Si(OH)_4$ value (+3.7 ‰) was found in surface waters at Sta. 2 (80°13'W) corresponding to highly depleted $Si(OH)_4$ concentrations of 0.4 μmol L^{-1} and high NO_3^-: $Si(OH)_4$ ratios (Figs 4, 5). In contrast, the highest $Si(OH)_4$ concentrations of >30 μmol L^{-1} are observed within the OMZ in bottom waters above the shelf (Sta. 807, 70 m to 109 m), which correspond to very low $\delta^{30}Si(OH)_4$ values (+ 1.1‰, Fig. 4c,d). Further offshore (Sta. 2, 3, 4, and 5) lower $Si(OH)_4$ concentrations (~10 to 20 μmol L^{-1}) at similar depths show intermediate $\delta^{30}Si(OH)_4$ signatures between +1.5‰ to +2.5‰, whereby the highest value below the oxycline was measured at Sta. 2 at a depth of 200m. NO_3^- concentrations range from 1.7 μmol L^{-1} to 33.9 μmol L^{-1} with $\delta^{15}NO_3^-$ ranging from + 3‰ to + 25‰. The lowest NO_3^- concentrations (1.7 μmol L^{-1} to 7 μmol L^{-1}) were found in surface waters and on the shelf at approximately 70m to 100m depth. Low NO_3^- concentrations are associated with the highest $\delta^{15}NO_3^-$ values of up to +25‰. Besides the shelf region and surface waters high $\delta^{15}NO_3^-$ values (+ 11‰ to + 16‰) are also observed at Sta. 5 (83°5'W) at 150 m water depth. Above the oxycline at 80°13'W (Sta. 2, center of the eddy) extremely low $\delta^{15}NO_3^-$ values (+3‰ to +5‰) were measured at 60 m to 80 m depth (Fig. 4f).

Surface waters along the 10°S transect

The highest $Si(OH)_4$ concentrations in the surface waters (10 μmol L^{-1}) can be found on the shelf at Sta. 807, from where $Si(OH)_4$ continuously decrease with distance from the shelf to less than 1 μmol L^{-1}. The highest surface water NO_3^- concentrations (21 μmol L^{-1}) were also measured on the shelf and show a decrease toward the open ocean, but still range between 2 μmol L^{-1} and 7 μmol L^{-1}, with the highest values occurring at Sta. 2, 4, and 5 (Fig. 5a). On the shelf at approximately 78°W, the lowest $\delta^{30}Si(OH)_4$ values

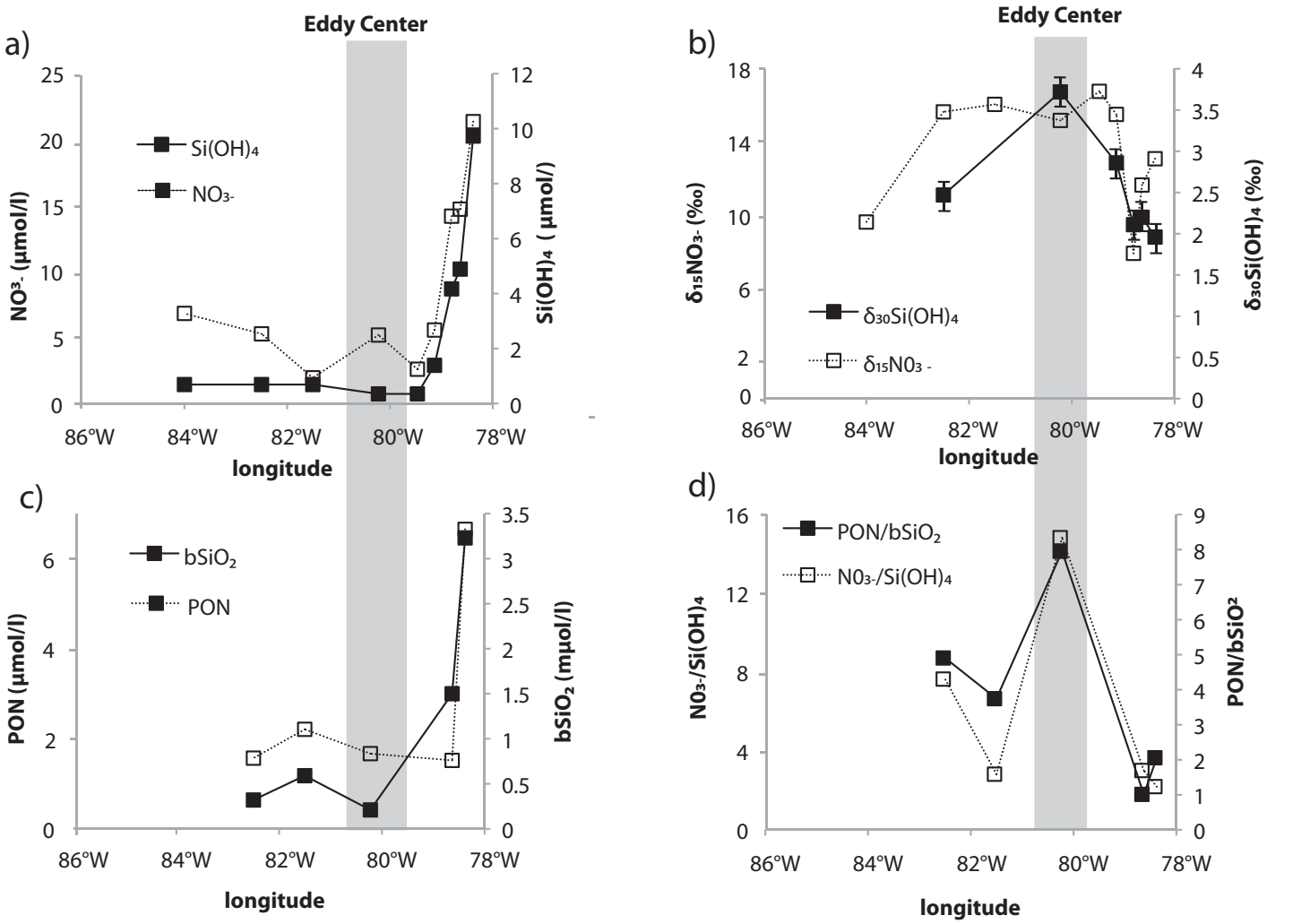

Fig. 5. (a) Surface distribution of $Si(OH)_4$ and NO_3^- concentrations, (b) $\delta^{30}Si(OH)_4$ and $\delta^{15}NO_3^-$ (2sd), the external error for $\delta^{15}NO_3^-$ is smaller than the symbols (c) $bSiO_2$ and PON concentrations and (d) NO_3^-: $Si(OH)_4$ ratios together with the ratios of the particulate phases (PON: $bSiO_2$). The gray shaded area indicates the extension of the inner center of the eddy structure (see also Figs. 1,3). PON and $bSiO_2$ were adapted from Franz et al. (2012).

(∼ + 2‰) were accompanied by relatively high $\delta^{15}NO_3^-$ signatures (+ 13‰). The highest $\delta^{30}Si(OH)_4$ value in surface waters in the center of the eddy (+3.7‰) correspond to a high $\delta^{15}NO_3^-$ signature of + 15‰, a very low $bSiO_2$ concentration (0.2 μmol L^{-1}), and the highest NO_3^-: $Si(OH)_4$ (∼15) and PON: $bSiO_2$ ratios (∼8) (Fig. 5c,d). Sta. 3 and Sta. 4 show high $\delta^{15}NO_3^-$ signatures (+16‰), whereas Sta. 5 is less fractionated (+10‰). In comparison, offshore Sta. 4 only shows moderately fractionated surface waters (+ 2.5‰) for $\delta^{30}Si(OH)_4$.

Rayleigh-type isotope fractionation model

To estimate the enrichment factors for Si and N isotopes in surface waters and within the OMZ, we applied a Rayleigh-type fractionation model (Supporting Information Fig. A3) in which the stable isotope compositions are related to the natural logarithm of the respective nutrient concentrations. A Rayleigh-type model describes a closed system, to which after a single input no additional nutrients are newly supplied (Mariotti et al., 1981). We are aware of the fact that the Raleigh-type model does not realistically describe the highly dynamic hydrographic system in the Peruvian upwelling system, which can be better approximated by a steady state model characterized by a continuous re-supply of nutrients (Ehlert at al., 2012). Along the 10°S transect this is, however, difficult to realize given that we have to assume an initial nutrient concentration for all stations. Based on the applied model we estimate an enrichment factor of −0.5‰ ($r^2 = 0.9$) for the surface water utilization of $Si(OH)_4$ (Supporting Information Fig. A3a). This model also shows that low $Si(OH)_4$ concentrations and high $\delta^{30}Si(OH)_4$ values (+ 3.7‰) also correspond to low nitrate concentrations and highest $\delta^{15}NO_3^-$ values (+ 16‰). For NO_3^- utilization an enrichment factor of −4.6‰ is estimated (Supporting

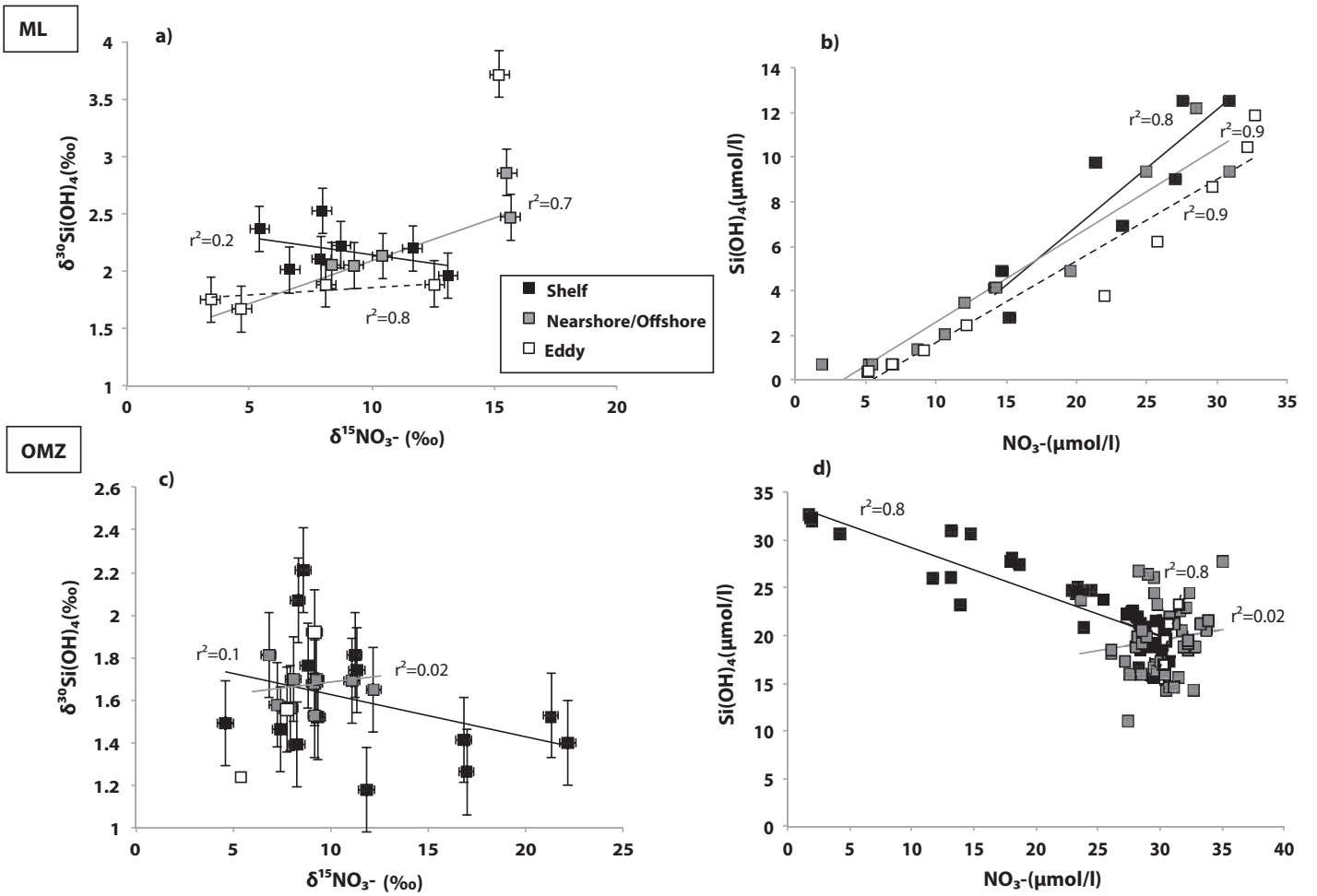

Fig. 6. Direct comparison between (a) $\delta^{30}Si(OH)_4$ and $\delta^{15}NO_3^-$, (b) $Si(OH)_4$ and NO_3^- concentrations in the ML where the water column is oxygenated. (c,d) stable isotope signatures and nutrient concentrations below the ML (max. depth of 300 m). This zone is characterized by oxygen concentrations below 5 μm L^{-1} (=OMZ). For all plots the data are divided in shelf samples (Sta. 807, Sta. 809, Sta. 810), nearshore and offshore samples (Sta. 812, Sta. 1, Sta. 3, Sta. 4, Sta. 5) as well as samples within the eddy center (Sta. 2).

Information Fig. A3b). The dissolved Si isotopes within the subsurface OMZ show a significantly weaker correlation to the nutrient concentrations ($r^2 = 0.5$) than the $\delta^{15}NO_3^-$ signatures ($r^2 = 0.8$), for which the model estimates an enrichment factor of −19.2‰ (Supporting Information Fig. A3c, d).

Comparison between silicon and nitrogen isotope compositions

The direct comparison between all $\delta^{30}Si(OH)_4$ and $\delta^{15}NO_3^-$ compositions, as well the corresponding concentrations for all samples (Fig. 6) indicates that the mixed layer (ML) at shelf stations (Sta. 807, 809, and 810) have negatively correlated stable $\delta^{30}Si(OH)_4$ and $\delta^{15}NO_3^-$ isotope signatures ($r^2 = 0.2$), where low $\delta^{15}NO_3^-$ (+5‰) correspond to high $\delta^{30}Si(OH)_4$ values (+ 2.5‰) and vice versa (Fig. 6a). Nearshore and offshore samples (Sta. 812, 1, 3, 4, 5) as well as samples from the eddy center (Sta. 2) are strongly positive correlated ($r^2 = 0.7$; $r^2 = 0.8$), if the surface value from the eddy center is excluded. The $\delta^{30}Si(OH)_4$ signatures of the samples from the eddy center (Sta. 2) are the same within error (~ + 1.8‰) while the $\delta^{15}NO_3^-$ values range from + 4‰ to 14‰. Only the surface sample in the eddy center differs markedly due to highly fractionated $\delta^{30}Si(OH)_4$ (+ 3.7‰). $Si(OH)_4$ and NO_3^- concentrations are positively correlated ($r^2 = 0.8$; $r^2 = 0.9$; $r^2 = 0.9$) with similar slopes for shelf and nearshore/offshore samples as well as the eddy center (Fig. 6b). The eddy center shows an enrichment in NO_3^- relative to $Si(OH)_4$. All sampling locations in the ML are rather limited by $Si(OH)_4$ rather than NO_3^- availability. Samples within the OMZ (<5 μmol L^{-1}) show no clear overall relationship between $\delta^{30}Si(OH)_4$ and $\delta^{15}NO_3^-$ (Fig. 6c). Some samples on the shelf show extremely high $\delta^{15}NO_3^-$ (+23‰) accompanied by low $\delta^{30}Si(OH)_4$ (+1.4‰), whereas other samples show a large range in $\delta^{30}Si(OH)_4$ (+1.4‰ to 2.2‰, but are relatively constant in $\delta^{15}NO_3^-$ [~+9‰]). In contrast, nutrient concentrations on the shelf are strongly negatively correlated

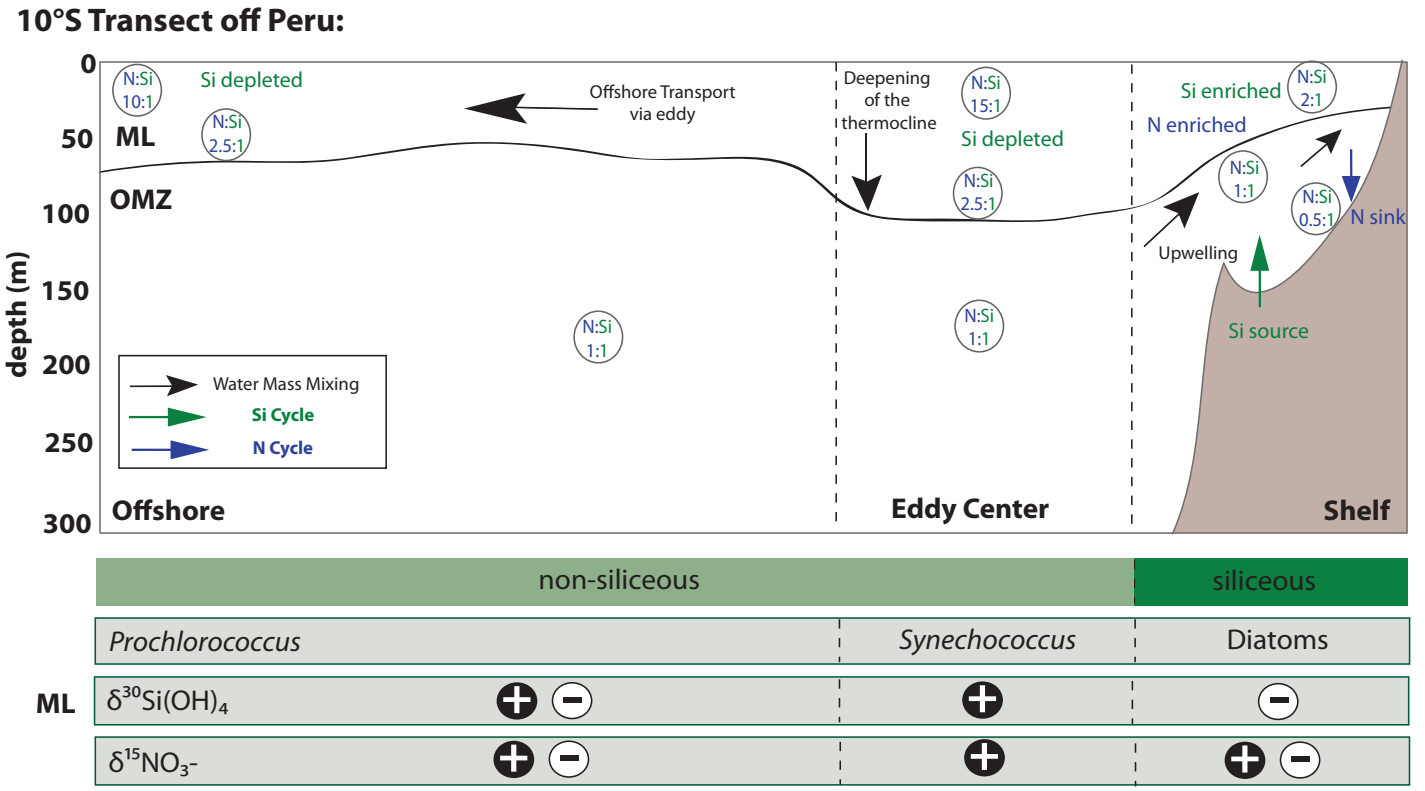

Fig. 7. Simplified schematic figure of the Si and N cycle along the 10°S transect for the ML and the OMZ. Water mass mixing processes (Eddy, upwelling) are indicated by black arrows. Processes within the Si cycle (green) and within the N cycle (blue) are shown in the figure together with the NO_3^- : $Si(OH)_4$ (N : Si) ratios. The transect is separated according to different hydrographic settings. Shelf stations (appr. 150 m water column depth) are influenced by strong upwelling together with processes at the sediment–seawater interface affecting the stable isotope composition. The center of the eddy shows a deeper stratification and is characterized by the highest $\delta^{30}Si(OH)4$ and $\delta^{15}NO_3$ values in surface waters together with the highest N: Si ratio. Below the schematic figure the dominant phytoplankton is given according to Franz et al. (2012). Siliceous Organisms (diatoms) are mainly dominant on the shelf, whereas non-siliceous organisms (Synechococcus, Prochlorococcus) dominate the eddy center and the offshore stations of the transect. For the main hydrographic regions also, the stable isotope composition in upper ML were classified as low $\delta^{30}Si(OH)$ values (~2‰, "minus sign"), moderate values ($\delta^{30}Si(OH)_4$ ~3‰; $\delta^{15}NO_3^-$ ~8 to 13‰; "minus and plus sign"), and high values ($\delta^{30}Si(OH)$ >3‰; $\delta^{15}NO_3^-$ ~14 to 16‰; "plus sign"). [Color figure can be viewed in the online issue, which is available at wileyonlinelibrary.com.]

Table 1. Parameters for the calculation of the Si IC in pore waters. Pore water depth within the sediment is given in cm. The depth of the southward PCUC as well as the bottom water depth is given in m in the water column.

Type	Station	Latitude	Depth	$Si(OH)_4$ μmol L^{-1}	$\delta^{30}Si(OH)_4$ ‰	*f*
Pore water	MUC26	10.75°S	0–1 cm	249.2	naN	0.0446
PCUC	Sta. 806	8°S	50–140 m	20	1.5	0.9554
Bottom water	Sta. 807	10°S	50–90 m	30.23	1.22	

($r^2 = 0.8$) with the lowest NO_3^- concentrations (2 μmol L^{-1}) corresponding to the highest $Si(OH)_4$ concentrations (33 μmol L^{-1}).

Discussion

We determined the upper water column distribution of $\delta^{30}Si(OH)_4$ and $\delta^{15}NO_3^-$ along a 10°S transect off Peru in order to better understand the processes controlling the $Si(OH)_4$ and NO_3^- cycling and the supply of these nutrients to the euphotic zone. The $Si(OH)_4$ and NO_3^- concentrations in surface waters and within the OMZ show a large variability, which is reflected differently by their stable isotope compositions as a function of water mass mixing and specific fractionation processes in the N and Si systems. In the following, we attempt to disentangle these processes along the 10°S transect and visualized them in a schematic diagram (Fig. 7).

Processes affecting the stable silicon and nitrogen isotope composition on the shelf

Sedimentary influence on the silicon cycle

The shelf stations differ markedly from those further offshore in terms of nutrient concentrations and stable isotope composition along the 10°S transect. They are characterized by the lowest $\delta^{30}Si(OH)_4$ values (+ 1.1‰) close to the bottom (110 m, Sta. 807) corresponding to high $Si(OH)_4$ concentrations of 33 μmol L^{-1} (Fig. 4). These elevated $Si(OH)_4$ concentrations are either a consequence of dissolution of $bSiO_2$ in the water column or of release from the sediments. In general, the dissolution of $bSiO_2$ in seawater is mainly controlled by physical parameters, such as temperature and pH (Lewin, 1961; Natori et al., 2006), but bacterial activity can lead to higher dissolution rates because it destroys the protecting organic layer of the diatom frustules (Bidle and Azam, 1999; Bidle et al., 2002). Given that bacterial activity is enhanced in OMZs (Diaz and Rosenberg, 2008; Ulloa et al., 2012), the dissolution of diatoms will be accelerated and may explain the pronounced increase in $Si(OH)_4$ and decrease in $\delta^{30}Si(OH)_4$ with depth. A previous field study by Grasse et al. (2013) in the EEP did, however, not find a clear link between $bSiO_2$ remineralization within the OMZ and the dissolved $\delta^{30}Si(OH)_4$. In addition, potential Si isotope fractionation during dissolution is still under discussion and might either have a low or neglectable effect (Demarest et al., 2009, Wetzel et al., 2014).

Elevated $Si(OH)_4$ concentrations are also visible within the southward flowing PCUC (Ehlert et al. 2012). From northern to southern Peru, $Si(OH)_4$ concentrations increase from 15 μmol L^{-1} to 40 μmol L^{-1}, which might be a combination of pore water inputs, dissolution of $bSiO_2$ in the water column and at the sediment-water interface. On the Peruvian shelf significant Si fluxes from the sediments to the overlying water column can be observed that are similar to observations from other upwelling areas. A time series study in Monterey Bay showed sedimentary Si fluxes between 3.06 mmol m^{-2} d^{-1} and 11.9 mmol m^{-2} d^{-1}, which varied seasonally and were tightly coupled to the rain rates of C_{org} and $bSiO_2$ (Berelson et al., 2003). This is in agreement with first results from the Peruvian shelf, where Si fluxes of up to 10 mmol m^{-2} d^{-1} were measured in benthic lander deployments (Noffke and Sommer pers. comm.) and pore water $Si(OH)_4$ concentrations were at the same time approximately 10 times higher (~250 μmol L^{-1}) than those of the bottom waters. To test the influence of pore water contributions, we apply a simple mixing model, for which we assumed that the water masses in 50 m to 90 m depth at Sta. 807 are only supplied by advection within the PCUC carrying a characteristic Si isotope signature of +1.5‰ ± 0.1‰ and a $Si(OH)_4$ concentration of 20 μmol L^{-1} obtained at stations north of 10°S (from Ehlert et al., 2012). The pore water concentration data (250 μmol L^{-1}) were taken from a set of multi corer data obtained during Meteor cruise M77-2 at 10°4′S (Noffke, 2014) (Table 1). This leads to a mixing relationship (Eq. 5) between the PCUC ($[Si]_{PCUC}$) and the pore water ($[Si]_{PW}$) end members contributing to the $Si(OH)_4$ concentration in bottom waters ($[Si]_{Bottom\ Water}$) (Table 1). The fractions (f) of the PCUC and the PW that are needed to explain the bottom water $Si(OH)_4$ concentration are calculated as follows

$$[Si]_{\mathrm{Bottom\ Water}} = \left([Si]_{\mathrm{PCUC}} * f\right) + \left([Si]_{\mathrm{PW}} * (1-f)\right) \quad (5)$$

Due to high $Si(OH)_4$ concentrations in pore waters their contribution is estimated to be only 4% whereas the remaining of 96% originate from the PCUC. Applying these calculated fractions to the water masses at Sta. 807 the Si isotope composition of pore waters can be estimated according to a two-endmember equation

$$\delta^{30}\mathrm{Si}_{\mathrm{Bottom\ Water}} = \frac{\left(\delta^{30}\mathrm{Si}_{\mathrm{PCUC}} * [\mathrm{Si}]_{\mathrm{PCUC}} * f\right) + \left(\delta^{30}\mathrm{Si}_{\mathrm{PW}} * [\mathrm{Si}]_{\mathrm{PW}} * (1-f)\right)}{\left([\mathrm{Si}]_{\mathrm{PCUC}} * f\right) + \left([\mathrm{Si}]_{\mathrm{PW}} * (1-f)\right)} \quad (6)$$

Equation solved for $\delta^{30}Si_{PW}$

$$\delta^{30}\mathrm{Si}_{\mathrm{PW}} = \frac{\delta^{30}\mathrm{Si}_{\mathrm{BW}}\left([\mathrm{Si}]_{\mathrm{PCUC}} * f\right) + \left([\mathrm{Si}]_{\mathrm{PW}} * (1-f)\right) - \left(\delta^{30}\mathrm{Si}_{\mathrm{PCUC}} * [\mathrm{Si}]_{\mathrm{PCUC}} * f\right)}{[\mathrm{Si}]_{\mathrm{PW}} * (1-f)} \quad (7)$$

According to this calculation a $\delta^{30}Si_{PW}$ signature of +0.7‰ on the shelf would be necessary to explain the light Si isotope signature in bottom waters (+ 1.2‰). This would imply that marine sediments characterized by high levels of $bSiO_2$ remineralization and high $Si(OH)_4$ fluxes are an important source for isotopically light Si. Unfortunately the Si fluxes from sediments are as yet not well constrained and have to be further investigated in order to arrive at better constrained estimates for the Peruvian shelf and for the marine Si budget in general (Tréguer and De LaRocha, 2013).

Processes controlling the nitrogen cycle on the shelf

The N cycle on the shelf is prominently characterized by diminished NO_3^- and elevated NO_2^- concentrations leading to distinctly elevated $\delta^{15}NO_3^-$ and $\delta^{15}NO_2^-$ signatures. The lowest NO_3^- concentrations (2 μmol L^{-1}) were found above the shelf and correspond to the highest $\delta^{15}NO_3^-$ values of up to +25‰ (Fig. 4e,f). $\delta^{15}NO_3^-$ is elevated within the OMZ due to denitrification and anammox processes, which have enrichment factors ranging from −20‰ to −30‰ (Brandes et al., 1998; Voss et al., 2001; Brunner et al., 2013) leaving the water column enriched in the heavy isotopes. On the basis of our $\delta^{15}NO_3^-$ data, it is not clearly distinguishable if the main N-loss processes are driven by anammox and/or denitrification. While a study by Kalvelage et al. (2013) found that anammox is the major process in the water column along the Peruvian shelf, the results of a study by Bohlen et al. (2011) showed that at the sediment-seawater

interface at 300 m to 1000 m water depth denitrification is the most important process along the Peruvian slope.

During the first step of the denitrification process NO_3^- is converted to NO_2^- associated with an increase of the $\delta^{15}N$ signature of the residual NO_3^- and a decrease of $\delta^{15}N$ signature of the NO_2^- produced. This can explain the very high NO_2^- concentrations of up to 11 μmol L^{-1} at Sta. 807 and supports denitrification to be the dominating process on the shelf, in particular at the sediment-seawater interface, but not the enriched $\delta^{15}NO_2^-$ values. Generally, the NO_2^- maxima found at deeper depths within the OMZ are associated with more negative $\delta^{15}NO_2^-$ values between −10‰ and 0‰, with NO_2^- concentrations ranging from 4 to 10 μmol L^{-1} (Casciotti et al., 2013). Interestingly, however, the $\delta^{15}NO_2^-$ shows the highest so far observed values (+15‰) at Sta. 807, which can only be explained by very efficient denitrification processes that transferred the highly positive $\delta^{15}N$ signal of the NO_3^- into the NO_2^- produced.

The N cycling on the Peruvian shelf is highly variable on short time scales and shows a tight coupling between different N processes. Overall, the shelf stations were obviously mainly influenced by sediment-seawater interactions, which led to a major decrease in NO_3^- and an increase in NO_2^- concentrations within the OMZ. Despite that NO_3^- concentrations are strongly depleted in the subsurface waters on the shelf as also indicated by low NO_3^-: $Si(OH)_4$ ratios (∼0.5), the surface waters are at the same time not depleted in NO_3^-, which is most likely caused by N recycling processes above the oxycline (NO_3^-: $Si(OH)_4$ ∼2.5) and admixture of other water masses (Fig. 7). In the following chapter, we will discuss the processes influencing the nutrients and the stable isotope signatures in the ML as well as the supply of water masses.

Processes in the mixed layer influenced by upwelling and the eddy circulation: silicon and nitrogen cycling

During utilization of $Si(OH)_4$ and NO_3^- lighter isotopes are preferentially incorporated into phytoplankton, resulting in heavier $\delta^{30}Si(OH)_4$ and $\delta^{15}NO_3^-$ values of seawater. The lowest $\delta^{30}Si(OH)_4$ values (+ 2.0‰ to + 2.2‰) in surface waters are observed on the shelf due to enhanced upwelling-derived supply of $Si(OH)_4$ with low $\delta^{30}Si(OH)_4$ signatures and therefore low utilization of the available $Si(OH)_4$ pool (Ehlert et al., 2012). These signatures correlate with elevated $\delta^{15}NO_3^-$ values (+ 8‰ to 13‰). According to the Raleigh-type model the calculated enrichment factors in surface waters are −0.5‰ for Si utilization and −4.6‰ for N utilization. This is in agreement with previous studies of the EEP, in which $^{30}\varepsilon/^{15}\varepsilon$ of −0.5‰ and −4.8‰, respectively, were estimated (Ehlert et al., 2012; Mollier-Vogel et al., 2012). Accordingly the source waters of these stations are expected to have $\delta^{30}Si(OH)_4$ signatures of ∼ + 1.5‰ and $\delta^{15}NO_3^-$ values of ∼ +5‰. Adopting an initial $\delta^{30}Si(OH)_4$ value for upwelled water in the shelf regions (mainly from the PCUC) of +1.5‰ (Ehlert et al., 2012), the surface water $\delta^{30}Si(OH)_4$ compositions can be fully explained. In contrast, $\delta^{15}NO_3^-$ signatures (∼ + 12‰) in surface waters are lower than in the subsurface source waters ($\delta^{15}NO_3^-$ ∼ + 20‰) and therefore suggest additional processes influencing the N isotope composition. One possible explanation is that the surface waters carrying a high subsurface signature were mixed with water masses carrying a lower $\delta^{15}NO_3^-$ signature of ∼ + 8‰ corresponding to waters with a potential density near 25.8 kg m^{-3}. This is in agreement with the $\delta^{30}Si(OH)_4$ signature of +2‰ at this density, which is essentially the same Si isotope value as the Si isotope signature of the surface waters (+2‰). In this case, the surface waters on the shelf are a mixture of two upwelling sources with only slightly different Si isotope signatures, where the constant resupply results in relatively unfractionated surface waters (Fig. 7).

Another possible explanation for the moderately fractionated $\delta^{15}NO_3^-$ signature in surface waters is intense remineralization of the high PON. This may also contribute to the isotope signature given that PON as remineralization may have lowered the $\delta^{15}N$ values by approx. 3‰ (Sigman et al., 2009, Möbius, 2013). Generally PON is more efficiently recycled (up to 70%) in the ML than $bSiO_2$ (∼ 50%) (Dugdale and Wilkerson, 1998; Demarest et al., 2011). The importance of remineralization in the surface waters has previously been demonstrated by a study of Fernandéz et al. (2009) who suggested that the surface waters off Peru are not only fuelled by "new" upwelled NO_3^- from below but that also "regenerated" N within the first meters of the water column plays an important role.

The availability of nutrients, influenced by water mass supply and remineralization also has a direct influence on the phytoplankton communities. During the sampling period, the dominating phytoplankton species in the eddy center where the thermocline deepened, stratification was stronger and surface waters were highly depleted in $Si(OH)_4$ compared to NO_3^- was *Synechococcus*, a picocyanobacterium (Franz et al., 2012; Fig. 7). Recently, Baines et al. (2012) discovered that *Synechococcus* can store high amounts of $Si(OH)_4$ and therefore can have a major influence on the marine Si cycle. So far, it is not known if the incorporation of $Si(OH)_4$ into *Synechococcus* is accompanied by significant Si isotope fractionation, but if so, the high abundance of *Synechococcus* could be the reason for the observed Si depletion. The high NO_3^-: $Si(OH)_4$ ratios (up to 15) therefore clearly point to the growth of non-siliceous organisms. Diatoms were most abundant in the ML on the shelf where low NO_3^-: $Si(OH)_4$ ratios (2.5) prevailed. Further offshore (Sta. 3, 4, 5), diatom productivity is reduced, as indicated by lower $bSiO_2$ and PON concentrations (0.6 μmol L^{-1}, respectively 2.2 μmol L^{-1}). These stations were characterized by moderately fractionated $\delta^{30}Si(OH)_4$ values (+2.5‰) and high $\delta^{15}NO_3^-$ (+16‰) most likely reflect the isotope composition of surface waters on the shelf, which are transported toward the offshore region via the eddy flow path and thereby are depleted in nutrients and heavier in their isotopic signals due to continuous utilization (a quasi-closed Rayleigh system; Figs. 1a, 5). NO_3^-: $Si(OH)_4$ ratios have a clear

influence on the phytoplankton communities, as already shown by a study from Vaillancourt et al. (2003) in the North Pacific that showed higher abundances of *Synechococcus* outside of a cyclonic eddy. Their cyclonic eddy was characterized by low NO_3^-: $Si(OH)_4$ ratios (~0.8) in its center and even lower NO_3^-: $Si(OH)_4$ ratios (~0.2) outside the eddy. In general, cyclonic eddies and mode water eddies inject nutrients from below into the euphotic zone while anticyclonic eddies decrease the nutrient content of the euphotic zone, which has also implications on the phytoplankton communities (e.g., Thompson et al., 2007; Bibby and Moore et al., 2011). Therefore, both the eddy types as well as the nutrient characteristics of the source waters clearly play an important role.

Stable isotope compositions and nutrient concentrations within the OMZ: Si and N cycling

The OMZ in the study area is characterized by oxygen concentrations below 5 μmol L^{-1}. The oxycline along the 10°S transect varied between 20 m and 90 m water depth closely following the 26.1 kg m^{-3} density surface and was strongly affected by the eddy, which caused a significant deepening of the oxycline at Sta. 2 (Fig. 4). The influence of the eddy on the nutrient distribution is therefore not only visible at the surface but also at greater depth (e.g., Altabet et al. 2012; Stramma et al., 2013). The variability of the distribution of the $Si(OH)_4$ concentrations closely correlates with density and therefore also the oxygen distribution. This is, however, not always directly mirrored by the Si isotope distribution. In general, the $\delta^{30}Si(OH)_4$ signatures in OMZ waters range between +1.5‰ and +2.3‰ (excluding Sta. 807) but do not reveal any clear correlation with the Si concentration or potential density. Therefore, we cannot clearly distinguish between isotopic changes as a consequence of $bSiO_2$ dissolution and water mass mixing. In contrast, the $\delta^{15}NO_3^-$ distribution clearly correlates with the NO_3^- concentration due to N-loss processes. NO_3^- reduction to NO_2^- is known to produce N and O isotopic fractionation with a characteristic slope near 1 (Granger et al., 2008). Deviations from this relationship have been interpreted as evidence for co-occurrence of other N transformation processes including NO_2^- oxidation and contributions from N_2 fixation (Sigman et al., 2005; Casciotti and McIlvin, 2007). For samples within the OMZ, the relationship between $\delta^{15}NO_3^-$ and $\delta^{18}O\text{-}NO_3^-$ along the 10°S transect is indistinguishable from a slope of 1 : 1 implying that is NO_3^- reduction is the main process. Applying a Rayleigh-type model an enrichment factor for N-loss of −19.2‰ was estimated within the OMZ, which is in agreement with published data from Casciotti (2009) and Ryabenko et al. (2012). However, a clear distinction if anammox or denitrification is the dominating process cannot be made.

Besides N-loss processes within the OMZ also nitrification occurs which ultimately generates NO_3^-. Generally, nitrification occurs in the aerobic waters, but a study by Ward et al. (1989) suggested that nitrification also takes place within the upper OMZ off Peru. Nitrification is associated with an inverse fractionation effect (~+13‰) (Casciotti and McIlvin, 2007; Casciotti, 2009) opposite in sign to the one expected for denitrification (~ −25‰) (Barford et al., 1999; Granger, 2006). A close coupling between denitrification and nitrification, could therefore result in the net elevated $\delta^{15}NO_3^-$ signatures given that the fractionation factor for denitrification is nearly double as high as the reverse one for nitrification (Casciotti, 2009).

Except for Sta. 5, which reveals elevated $\delta^{15}NO_3^-$ values (+16‰) at 150 m depth, the $\delta^{15}NO_3^-$ values in the study area are relatively homogenous at +8‰ to +10‰ and therefore only moderately fractionated within the OMZ (Fig. 4f). The elevated $\delta^{15}NO_3^-$ values at Sta. 5 may thus represent a signal that originated on the shelf as also indicated by the data of Altabet et al. (2012), which showed $\delta^{15}NO_3^-$ values up to +40‰ at the end of the outermost offshore filament of the eddy. In general, NO_3^- concentrations within the anticyclonic eddy are still relatively high (~25 μmol L^{-1}) compared with another anticyclonic mode water eddy south of our study area (~16°S), which showed extremely high $\delta^{15}NO_3^-$ values (up to +70‰ in its center) and highly depleted nitrate concentrations (Bourbonnais et al., 2015). These authors therefore suggested that eddies are "N-loss Hotspots." At 16°S NO_3^- concentrations are generally lower, which is also indicated by very low N* values (Zamora et al., 2012) compared to our study area. However, the anticyclonic eddy investigated in our study rather suggests that these eddies are not generally "N-loss hotspots" and shows that their influence on biogeochemical cycling of nutrients is highly dependent on the history of their source waters.

Factors controlling the silicon and nitrogen cycle in the Peruvian Upwelling: what can we learn from the combination of silicon and nitrogen isotopes

In this study, the first direct comparison between the distributions of dissolved $\delta^{30}Si(OH)_4$ and $\delta^{15}NO_3$ in the OMZ of the Peruvian Upwelling area serves to better understand the factors controlling the biogeochemical cycling of both nutrients (Fig. 7). Samples were taken along a 10°S transect perpendicular to the Peruvian coast and therefore covered a large range of different hydrographic settings including strong upwelling and locations influenced by the eddy. Upwelling as well as the eddy had a large influence on the $Si(OH)_4$ and NO_3^- concentrations, as well as on the corresponding isotopes. Along with the Eddy nutrients were transported offshore and our data are consistent with continuous utilization along the transport pathway, which especially led to Si depleted waters offshore. In contrast, even though N-loss processes within the OMZ diminished the NO_3^- concentrations, NO_3^- was never completely utilized in surface waters. This was due to efficient recycling and re-supply of NO_3^- within the upper water column (above the OMZ), which is reflected by the stable isotopes confirming that N is more efficiently recycled in the upper water column than Si. The higher regeneration efficiency of N is also traceable by the pronounced Si deficit (Si*) above the oxycline. Very low

NO_3^-: $Si(OH)_4$ (<1) was found in bottom waters on the shelf, where the highest $\delta^{15}NO_3^-$ (+25‰) values were accompanied by the lowest $\delta^{30}Si(OH)_4$. There we also found a strong negative coupling between $Si(OH)_4$ and NO_3^- concentrations, most likely because the organic matter fueling the N-loss processes is derived from sinking diatoms. Our study shows that in upwelling regions, which are characterized by high productivity, decomposition of organic matter and therefore a pronounced OMZ, the Si and N cycles are strongly linked: surface waters on the shelf influenced by strong upwelling show a negative coupling between Si and N isotopes (low $\delta^{30}Si(OH)_4$, high $\delta^{15}NO_3^-$), whereas stations further offshore are positively coupled (high $\delta^{30}Si(OH)_4$, high $\delta^{15}NO_3^-$).

The information we gain from a combined approach using $\delta^{30}Si(OH)_4$ and $\delta^{15}NO_3^-$ isotope data not only helps to understand recent biogeochemical processes but also helps to reconstruct biogeochemical cycling in the past. N-loss processes can influence the $\delta^{15}N$ signature of sedimentary record, given that supply of the heavy $\delta^{15}NO_3^-$ signatures from subsurface waters leads to PON enriched in ^{15}N, which is ultimately buried in the sediments (e.g., Altabet et al., 1994; Altabet, 2006; Mollier-Vogel et al., 2012). In general, the $\delta^{15}N$ obtained from sediment cores in OMZs are usually interpreted to directly reflect changes in the intensity of subsurface N-loss and the extent and strength of oxygen depletion (e.g., De Pol-Holz et al. 2007; Guitíerrez et al. 2009), whereas the effect of NO_3^- utilization is often neglected. The combined approach shows that surface waters influenced by strong upwelling are characterized by low $\delta^{30}Si(OH)_4$ values (+2‰) due to low Si utilization but relatively high $\delta^{15}NO_3^-$ (+13‰) values due to upwelling of waters influenced by N-loss processes. In sedimentary records $\delta^{15}N$ would rather result from a N-loss signal. In contrast, $Si(OH)_4$ and NO_3^- concentrations and the corresponding stable isotope signatures are strongly positively correlated within the surface ML at nearshore and offshore stations including regions where siliceous organisms are not dominating the phytoplankton community (Fig. 7). A positive correlation between $\delta^{30}Si$ and $\delta^{15}N$ would thus indicate that the signal preserved in sediments is derived from utilization processes of both nutrients. A recent study by Ehlert et al. (2015) already used the combined approach of both stable isotope obtained from sediment cores and concluded that during the past $\sim$ 650 years $\delta^{15}N$ has to a large extend been controlled by utilization of NO_3^- and not by N-loss processes as previously suggested. In upwelling areas where the Si and N cycles are closely linked, the dual isotope approach using Si and N isotopes will therefore lead to a better understanding of present and past biogeochemical processes and help to identify source waters.

References

Altabet, M. A. 2001. Nitrogen isotopic evidence for micronutrient control of fractional NO_3^- utilization in the equatorial Pacific. Limnol. Oceanogr. **46**: 368–380.

Altabet, M. A. 2006. Isotopic tracers of the marine nitrogen cycle, p. 251–293. *In* J. Volkman, [ed.], Marine organic matter: Chemical and biological markers, 2. Springer-Verlag, Berlin Heidelberg.

Altabet, M. A., and R. Francois, R. 1994. Sedimentary nitrogen isotopic ratio as a tracer for surface ocean nitrate utilization. Global Biogeochem. Cycles **8**: 103–116.

Altabet, M. A., E. Ryabenko, L. Stramma, D. W. R. Wallace, M. Frank, P. Grasse, and G. Lavik. 2012. An eddy-stimulated hotspot for fixed nitrogen-loss from the Peru oxygen minimum zone. Biogeosciences **9**: 4897–4908.

Ayon, P., M. I. Criales-Hernandez, R. Schwamborn, and H. Hirche. 2008. Zooplankton research off Peru: A review. Prog. Oceanogr. **79**, 238–255.

Barford, C., J. P. Montoya, M. A., Altabet, and R. Mitchell. 1999. Steady-state nitrogen isotope effects of N_2 and N_2O production in Paracoccus denitrificans. Appl. Environ. Microbiol. **65**: 9889–9994.

Baines, S. B., B. S. Twining, M. A. Brzezinski, J. W., Krause, S. Vogt, D. Assael, and H. McDaniel. 2012. Significant silicon accumulation by marine picocyanobacteria. Nat. Geosci. **5**: 886–891

Berelson, W., and others. 2003. A time series of benthic flux measurements from Monterey Bay, CA. Cont. Shelf Res. **23**: 457–481.

Berger, W. H., V. S. Smetacek, and G. Wefer. 1989. Productivity of the ocean: Present and past, p. 471. Wiley.

Bibby, T. S., and C. M. Moore. 2011. Silicate:nitrate ratios of upwelled waters control the phytoplankton community sustained by mesoscale eddies in sub-tropical North Atlantic and Pacific. Biogeosciences **8**: 657–666.

Bidle, K. D., and F. Azam. 1999. Accelerated dissolution of diatom silica by marine bacterial assemblages. Nature **397**: 508–512.

Bidle, K. D., M. Manganelli, and F. Azam. 2002. Regulation of oceanic silicon and carbon preservation by temperature control on bacteria. Science **298**: 1980–1983.

Bourbonnais, A., M. A. Altabet, C. N. Charoenpong, J. Larkum, H. Hu, H. W. Bange, and L. Stramma. 2015. N-loss isotope effects in the Peru oxygen minimum zone studied using a mesoscale eddy as a natural tracer experiment. Global Biogeochem. Cycles **29**: 793–811.

Brandes, J. A., A. H. Devol, T. Yoshinari, D. A. Jayakumar, and W. A. Naqvi. 1998. Isotopic composition of nitrate in the central Arabian Sea and eastern tropical North Pacific: A tracer for mixing and nitrogen cycles. Limnol. Oceanogr. **43**: 1680–1689.

Brink, K., D. Halpern, A. Huyer, and R. L. Smith. 1983. The physical environment of the Peruvian upwelling system. Prog. Oceanogr. **12**: 285–305.

Bruland, K., E. Rue, G. Smith, and G. Ditullio. 2005. Iron, macronutrients and diatom blooms in the Peru upwelling regime: Brown and blue waters of Peru. Mar. Chem. **93**: 81–103.

Brunner, B., and others. 2013. Nitrogen isotope effects induced by anammox bacteria. Proc. Natl. Acad. Sci. USA **110**: 18994–18999.

Brzezinski, M. A. 1985. The Si:C:N ratio of marine diatoms_interspecific variability and the effect of some environmental variables. J. Phycol. **21**: 347–357.

Bohlen, L., and others. 2011. Benthic nitrogen cycling traversing the Peruvian oxygen minimum zone. Geochim. Cosmochim. Acta **75**: 6094–6111.

Casciotti, K. L. 2009. Inverse fractionation during bacterial nitrite oxidation. Geochim. Cosmochim. Acta **73**: 2061–2076

Casciotti, K. L., and M. R. Mcllvin. 2007. Isotopic analyses of nitrate and nitrite from references mixtures and application to Eastern Tropical North Pacific waters. Mar. Chem. **107**: 184–201.

Casciotti, K. L., C. Buchwald, and M. McIlvin. 2013. Implications of nitrate and nitrite isotopic measurements for the mechanisms of nitrogen cycling in the Peru oxygen deficient zone. Deep-Sea Res. Part I **80**: 78–93

Chaigneau, A., A. Gizolme, and C. Grados. 2008. Mesoscale eddies off Peru in altimeter records: Identification algorithms and eddy spatio-temporal patterns. Prog. Oceanogr. **79**: 106–119.

Codispoti, L. A. 2007. An oceanic fixed nitrogen sink exceeding 400 Tg N a−1 vs. the concept of homeostasis in the fixed-nitrogen inventory. Biogeosciences **4**: 233–253.

Conley, D. J., and T. C. Malone. 1992. Annual cycle of dissolved silicate in Chesapeake Bay: Implications for the production and fate of phytoplankton biomass. Mar. Ecol. Prog. Ser. **81**: 121–128.

Czeschel, R., L. Stramma, F. U. Schwarzkopf, B. S. Giese, A. Funk, and J. Karstensen. 2011. Mid-depth circulation of the eastern tropical South Pacific and its link to the oxygen minimum zone. J. Geophys. Res. **116**: C01015. doi: 10.1029/2010JC006565

De LaRocha, C., M. A. Brzezinski, and M. DeNiro. 1997. Fractionation of silicon isotopes by marine diatoms during biogenic silica formation. Geochim. Cosmochim. Acta **61**: 5051–5056.

Demarest, M. S., M. A. Brzezinski, and C. P. Beucher. 2009. Fractionation of silicon isotopes during biogenic silica dissolution. Geochim. Cosmochim. Acta **73**: 5572–5583.

Demarest, M. S., M. A. Brzezinski, D. M. Nelson, J. W. Krause, J. L. Jones, and C. P. Beucher. 2011. Net biogenic silica production and nitrate regeneration determine the strength of the silica pump in the Eastern Equatorial Pacific. Deep-Sea Res. Part II **58**: 462–476.

De Pol-Holz, R., O. Ulloa, F. Lamy, L. Dezileau, P. Sabatier, and D. Hebbeln. 2007. Late Quaternary variability of sedimentary nitrogen isotopes in the eastern South Pacific Ocean. Paleoceanography **22**: PA2207. doi:10.1029/2006PA001308

Deutsch, C., J. L. Sarmiento, D. M. Sigman, N. Gruber, and J. P. Dunne. 2007. Spatial coupling of nitrogen inputs and losses in the ocean. Nature **445**: 164–167.

Diaz, R. J. R., and R. R. Rosenberg. 2008. Spreading dead zones and consequences for marine ecosystems. Science **321**: 926–929.

Dugdale, R. C., and F. P. Wilkerson. 1998. Silicate regulation of new production in the equatorial Pacific upwelling. Nature **391**: 270–273.

Ehlert, C., and others. 2012. Factors controlling the silicon isotope distribution in waters and surface sediments of the Peruvian coastal upwelling. Geochim. Cosmochim. Acta **99**: 128–145

Ehlert, C., P. Grasse, D. Guitiérrez, R. Salvatteci, and M. Frank. 2015. Nutrient utilisation and weathering inputs in the Peruvian upwelling region since the Little Ice Age. Clim. Past **11**: 1–16.

Estrada, M., and D. Blasco. 1985. Phytoplankton assemblages in coastal upwelling areas, p. 379–402. *In* C. Bas, R. Margalef, and P. Rubies [eds.], Simposio Internacional Sobre Las Areas de Afloramiento Mas Importantes del Oeste Africano (Cabo Blanco y Benguela). Instituto de Investigaciones Pesqueras.

Fernández, C., L. Farías, and M. E. Alcaman. 2009. Primary production and nitrogen regeneration processes in surface waters of the Peruvian upwelling system. Prog. Oceanogr. **83**: 159–168.

Fiedler, P., and L. Talley. 2006. Hydrography of the eastern tropical Pacific: A review. Prog. Oceanogr. **69**: 143–180.

Franck, V. M., M. A. Brzezinski, K. H. Coale, and D. M. Nelson. 2000. Iron and silicic acid concentrations regulate Si uptake north and south of the Polar Frontal Zone in the Pacific Sector of the Southern Ocean. Deep-Sea Res. Part II **47**: 3315–3558

Franz, J., G. Krahmann, G. Lavik, P. Grasse, P. Dittmar, and U. Riebesell. 2012. Dynamics and stoichiometry of nutrients and phytoplankton in waters influenced by the oxygen minimum zone in the eastern tropical Pacific. Deep-Sea Res. Part I **62**: 20–31

Fuenzalida, R., W. Schneider, J. Garcés-Vargas, L. Bravo, and C. Lange, C. 2009. Vertical and horizontal extension of the oxygen minimum zone in the eastern South Pacific Ocean. Deep Sea Res. Part II **56**: 992–1003.

Georg, R. B., B. Reynolds, M. Frank, and A, Halliday. 2006. New sample preparation techniques for the determination of Si isotopic compositions using MC-ICPMS. Chem. Geol. **235**: 95–104.

Granger, J., D. M. Sigman, J. A. Needoba, and P. J. Harrison. 2004. Coupled nitrogen and oxygen isotope fractionation of nitrate during assimilation by cultures of marine phytoplankton. Limnol. Oceanogr. **49**: 1763–1773.

Granger, J., D. M. Sigman, M. F. Lehmann, and P. D. Tortell. 2008. Nitrogen and oxygen isotope fractionation during dissimilatory nitrate reduction by denitrifying bacteria. Limnol. Oceanogr. **53**: 2533.

Granger, J., D. Sigman, and M. Rohde. 2010. N and O isotope effects during nitrate assimilation by unicellular

prokaryotic and eukaryotic plankton cultures. Geochim. Cosmochim. Acta **74**: 1030–1040.

Grasse, P., T. Stichel, R. Stumpf, L. Stramma, and M. Frank, M. 2012. The distribution of neodymium isotopes and concentrations in the Eastern Equatorial Pacific Water mass advection versus particle exchange. Earth Planet. Sci. Lett. **353–354**: 198–207.

Grasse, P., C. Ehlert, and M. Frank. 2013. The influence of water mass mixing on the dissolved Si isotope composition in the Eastern Equatorial Pacific. Earth Planet. Sci. Lett. **380**: 60–71.

Grasshoff, K., K. Kremlin, and M. Erhardt. 1999. Methods for seawater analysis – third completely revised and extended version, p. 600. Wiley VHC.

Gruber, N., Z. Lachkar, H. Frenzel, P. Marchesiello, M. Münnich, J. C. McWilliams, T. Nagai, and G.-K. Plattner. 2011. Eddy-induced reduction of biological production in eastern boundary upwelling systems. Nat Geosci. **4**: 787–792.

Gutiérrez, D., and others. (2009). Rapid reorganization in ocean biogeo- chemistry off Peru towards the end of the Little Ice Age. Biogeosciences **6**: 835–848. doi:10.5194/bg-6-835-2009

Hutchins, D. A., and K. W. Bruland. 1998. Iron-limitated diatom growth and Si:N uptake ratios in a coastal upwelling regime. Nature **393**: 561–563

Huyer, A., R. L. Smith, and T. Paluszkiewicz. 1987. Coastal Upwelling off Peru During Normal and El Niño Times, 1981–1984. J Geophys. Res. **92**: 14.297–14.307. doi: 10.1029/JC092iC13p14297

Kalvelage, T., and others. 2013. Nitrogen cycling driven by organic matter export in the South Pacific oxygen minimum zone. Nat. Geosci. **6**: 228–234.

Karl, D. M., and G. Tien. 1992. MAGIC: A sensitive and precise method for measuring dissolved phosphorus in aquatic environments. Limnol. Oceanogr. **37**: 105–116.

Karstensen, J. 2004. Formation of the South Pacific Shallow Salinity Minimum: A Southern Ocean Pathway to the Tropical Pacific. J. Phys. Oceanogr. **34**: 2398. doi:10.1175/JPO2634.1

Karstensen, J., and O. Ulloa. 2008. The Peru-Chile Current System. Encyclopedia of Ocean Sciences 2nd edition online.

Karstensen, J., L. Stramma, and M. Visbeck. 2008. Oxygen minimum zones in the eastern tropical Atlantic and Pacific oceans. Prog. Oceanogr. **77**: 331–350.

Kessler, W. 2006. The circulation of the eastern tropical Pacific: A review. Prog. Oceanogr. **69**: 181–217.

Lam, P., and others. 2009. Revising the nitrogen cycle in the Peruvian oxygen minimum zone. Proc. Natl. Acad. Sci. USA **106**: 4752–4757.

Lewin, J. 1961. The dissolution of silica from diatom walls. Geochim. Cosmochim. Acta **21**: 182–198.

Mariotti, A., J. Germon, P. Hubert, P. Kaiser, R. Letolle, A. Tardieux, and P. Tardieux. 1981. Experimental-Determination of nitrogen kinetic isotope fractionation – some principles – illustration for the denitrification and nitrification processes. Plant Soil **62**: 413–430.

McGillicuddy, D., A. Robinson, and D. Siegel. 1998. Influence of mesoscale eddies on new production in the Sargasso Sea. Nature **394**: 263–266.

McIlvin, M. R. and M. A. Altabet. 2005. Chemical conversion of nitrate and nitrite to nitrous oxide for nitrogen and oxygen isotopic analysis in freshwater and seawater. Anal. Chem. **77**: 5589–5595.

Milligan, A. J., D. E. Varela, M. A., Brzezinski, and F. M. M. Morel. 2004. Dynamics of silicon metabolism and silicon isotopic discrimination in a marine diatom as a function of pCO2. Limnol. Oceanogr. **49**: 322–329.

Möbius, J. 2013. Isotope fractionation during nitrogen remineralization (ammonification): Implications for nitrogen isotope biogeochemistry. Geochim. Cosmochim. Acta **105**: 422–432.

Mollier-Vogel, E., E. Ryabenko, P. Martinez, D. Wallace, M. A. Altabet, and R. Schneider. 2012. Nitrogen isotope gradients off Peru and Ecuador related to upwelling, productivity, nutrient uptake and oxygen deficiency. Deep-Sea Res. Part I **70**: 14–25.

Montoya, J. P. and J. J. McCarthy. 1995. Isotopic fractionation during nitrate uptake by phytoplankton grown in continuous culture. J Plankton Res. **17**: 439–464.

Natori, Y., A. Haneda, and Y. Suzuki. 2006. Vertical and seasonal differences in biogenic silica dissolution in natual seawater in Surunga Bay, Japan: Effects of temperature and organic matter. Mar. Chem. **102**: 230–241.

Needoba, J. A., N. A. Waser, P. J., Harrison, and S. E. Calvert. 2003. Nitrogen isotope fractionation in 12 species of marine phytoplankton during growth on nitrate. Mar. Ecol. Prog. Ser. **255**: 81–91.

Nelson, D., P. Tréguer, M. A. Brzezinski, A. Leynaert, and B. Queguiner. 1995. Production and dissolution of biogenic silica in the ocean: Revised global estimates, comparison with regional data and relationship to biogenic sedimentation. Global Biogeochem. Cycles **9**: 359–372.

Noffke, A. 2014. Phosphorus Cycling in anoxic sediments. Ph. D. thesis. Christian-Albrecht University Kiel.

Pennington, J. T., K. Mahoney, V. Kuwahara, D. Kolber, R. Calienes, and F. P. Chavez. 2006. Primary production in the eastern tropical Pacific: A review. Prog. Oceanogr. **69**: 285–317.

Penven, P., V. Echevin, J. Pasapera, F. Colas, and J. Tam. 2005. Average circulation, seasonal cycle, and mesoscale dynamics of the Peru Current System: A modeling approach. J. Geophys. Res. **110**: C1002. doi: 10.1029/2005JC002945

Ragueneau, O., and others. 2000. A review of the Si cycle in the modern ocean: Recent progress and missing gaps in the application of biogenic opal as a paleoproductivity proxy. Global Planet. Change **26**: 317–365.

Reid, J. 1973. The shallow salinity minima of the Pacific Ocean. Deep-Sea Res. **20**: 51–68.

Reynolds, B., M. Frank, and A. Halliday. 2006. Silicon isotope fractionation during nutrient utilization in the North Pacific. Earth Planet. Sci. Lett. **244**: 431–443.

Ryabenko, E., M. A. Altabet, and D. W. R. Wallace. 2009. Effect of chloride on the chemical conversion of nitrate to nitrous oxide for $\delta^{15}N$ analysis. Limnol. Oceanogr.: Methods **7**: 545–552.

Ryabenko, E., A. Kock, H. W. Bange, M. A. Altabet, and D. W. R. Wallace. 2012. Contrasting biogeochemistry of nitrogen in the Atlantic and Pacific oxygen minimum zones. Biogeosciences **9**: 203–212

Sigman, D. M., J. Granger, P. J., DiFiore, M. M. Lehmann, R. Ho, G. Cane, and A. van Geen, A. 2005. Coupled nitrogen and oxygen isotope measurements of nitrate along the eastern North Pacific margin. Global Biogeochem. Cycles **19**: GB4022.

Sigman, D. M., K. L. Karsh, and K. L. Casciotti. 2009. Ocean process tracers: Nitrogen isotopes in the ocean. Encyclopedia of ocean science, 2nd edn. Elsevier.

Stramma, L., H. W. Bange, R. Czeschel, A. Lorenzo, and M. Frank. 2013. On the role of mesoscale eddies for the biological productivity and biogeochemistry in the eastern tropical Pacific Ocean off Peru. Biogeosciences **10**: 7293–7306.

Strickland, J. D. H., O. Holm-Hansen, R. W. Eppley, and R. J. Linn. 1969. The use of a Deep Tank in Plankton Ecology. I. Studies of the growth and composition of Phytoplankton Crops at Low Nutrient Levels. Limnol. Oceanogr. **14**: 23–34.

Strub, P. T., J. M. Mesías, V. Montecino, and J. Rutllant. 1998. Coastal Ocean Circulation off Western South America. Sea **11**: 273–313.

Sutton, J., D. E. Varela, A. Brzezinski, and C. P. Beucher. 2012. Species-dependent silicon isotope fractionation by marine diatoms. Geochim. Cosmochim. Acta **104**: 300–309.

Thiede, J., and E. Suess. 1983. Coastal upwelling: Its sediment record, p. 610. Plenum Publishing Corporation.

Thomas, W. H. 1979. Anomalous nutrient-chlorophyll interrelationships in the offshore eastern tropical Pacific Ocean. J. Mar. Res. **37**: 327–335.

Thompson, P. A., S. Pesant, and A. W. Waite. 2007. Contrasting the vertical differences in the phytoplankton biology of a dipole pair of eddies in the south-eastern Indian Ocean. Deep-Sea Res. Part II **54**: 1003–1028.

Toggweiler, J. R., K. Dixon, and W. S. Broecker. 1991. The Peru Upwelling and the Ventilation of the South Pacific Thermocline. J. Geophys. Res. **96**: 467–497. doi:10.1029/91JC02063

Tréguer, P. J., and C. L. De LaRocha. 2013. The World Ocean Silica Cycle. Annu. Rev. Mar. Sci. **5**: 477–501.

Ulloa, O., D. E. Canfield, E. F. DeLong, R. M. Letelier, and F. J. Stewart. 2012. Microbial oceanography of anoxic oxygen minimum zones. Proc Natl Acad Sci USA **109**: 15996–16003.

Vaillancourt, R. D., J. Marra, M. P. Seki, M. L. Parsons, and R. R. Bidigare. 2003. Impact of a cyclonic eddy on phytoplankton community structure and photosynthetic competency in the subtropical North Pacific Ocean. Deep-Sea Res. Part I **50**: 829–847.

Voss, M., J. W. Dippner, and J. P. Montoya. 2001. Nitrogen isotope patterns in the oxygen-deficient waters of the Eastern Tropical North Pacific Ocean. Deep-Sea Res. Part I **48**: 1905–1921.

Wada, E. 1980. Nitrogen isotope fractionation and its significance in biogeochemical processes occurring in marine environments, p. 375–398. *In* E. Goldberg, Y. Horibe, and K. Saru- hashi [eds.], Isotope Marine Chemistry. Uchida Rokakuho.

Ward B. B., Glover, H. E., & Lipschultz, F. 1989. Chemoautotrophic activity and nitrification in the oxygen minimum zone off Peru. Deep Sea Research Part A. Oceanographic Research Papers, **36**(7), 1031–1051.

Wetzel, F., G. F. de Souza, and B. C. Reynolds. 2014. What controls silicon isotope fractionation during dissolution of diatom opal? Geochim. Cosmochim. Acta **131**: 128–137.

Wilkerson, F. P., and R. C. Dugdale. 1996. Silicate versus nitrate limitation in the equatorial Pacific estimated from satellite-derived sea-surface temperatures. Adv. Space Res. **18**: 81–89.

Winkler, L. W. 1888. Die Bestimmung des im Wasser gelösten Sauerstoffs. Ber. Dtsch Chem. Ges. **21**: 2843–2855.

Zamora, L. M., A. Oschlies, H. W. Bange, K. B. Huebert, J. D. Craig, A. Kock, and C. R. Löscher. 2012. Nitrous oxide dynamics in low oxygen regions of the Pacific: Insights from the MEMENTO database. Biogeosciences **9**: 5007–5022.

Acknowledgments

Special thanks go to the crew of the R/V Meteor for their support during cruise M77/3. We also like to thank the editors of Limnology and Oceanography Anya Waite and Robert Howarth and two anonymous reviewers for their constructive comments, which helped to improve the manuscript. This work is a contribution of the Sonderforschungsbereich 754 "Climate–Biogeochemistry Interactions in the Tropical Ocean" (www.sfb754.de) funded by the Deutsche Forschungsgemeinschaft.

Submitted 3 February 2015
Revised 31 July 2015; 23 Nov 2015; 7 Feb 2016
Accepted 11 April 2016

Associate editor: Anya Waite